SANDIA REPORT

SAND89—1196 • UC—703
Unlimited Release
Printed September 1989

The Effect of Strain Rate on the Compressive Strength of Dry and Saturated Tuff

William A. Olsson

Prepared by
Sandia National Laboratories
Albuquerque, New Mexico 87185 and Livermore, California 94550
for the United States Department of Energy
under Contract DE-AC04-76DP00789

Issued by Sandia National Laboratories, operated for the United States Department of Energy by Sandia Corporation.

Available to DOE and DOE contractors from
Office of Scientific and Technical Information
PO Box 62
Oak Ridge, TN 37831

Prices available from (615) 576-8401, FTS 626-8401

Available to the public from
National Technical Information Service
US Department of Commerce
5285 Port Royal Rd
Springfield, VA 22161

NTIS price codes
Printed copy: A02
Microfiche copy: A01

Distribution
Category UC-703

SAND89-1196
Unlimited Release
Printed September 1989

SAND--89-1196

DE90 000854

The Effect of Strain Rate on the Compressive Strength of Dry and Saturated Tuff

William A. Olsson

Geomechanics Division
Sandia National Laboratories
Albuquerque, New Mexico 87185

ABSTRACT

The uniaxial compressive strength of air-dry and water-saturated ashfall tuff from the Nevada Test Site was measured as a function of strain rate from 10^{-6} to 10^{3} s^{-1} . Two different testing devices were used to achieve this wide range in rate, an electro-hydraulic, servo-controlled load frame, and a Kolsky bar. Critical strain rates of 82 s^{-1} and 22 s^{-1} were found for dry and saturated tuffs, respectively. Below the critical rate the strength is a weak function of strain rate and above the critical rate strength varies as the cube root of strain rate. The strengths of the dry and saturated tuff are the same above the critical rate. At slower rates, the saturated tuff is weaker at all rates and shows a slightly stronger strain-rate sensitivity.

---

*This work performed at Sandia National Laboratories supported by the U.S. Department of Energy under contract number DE-AC04-76DP00789.

Contents

List of Figures

1 Introduction

The influence of strain rate on the mechanical response of rocks is of interest for several reasons. The data are needed in calculations to predict such things as ground motion and containment of gases in explosively formed underground cavities, and fragment sizes and distributions caused by percussive or explosive rock fragmentation. From a more general perspective, the development of complete micromechanical or physical theories of rock deformation requires data over the widest possible range in strain rates. It is probable that rocks suffer deformations over a wider range of rates than any other material. Slow earth deformations take place at rates down to around 10^{-16} s^{-1} . On the other end of the scale, meteorite impacts and nuclear explosions can generate strain rates in excess of 10^{8} s^{-1} . The rates reported here cover an intermediate range of 10^{-6} to 10^{3} s^{-1} .

2 Experimental Procedures

Two different testing systems were used to achieve the wide range of strain rate reported in this paper. Uniaxial compression tests at room temperature and at strain rates from 10^{-6} to 4 s^{-1} were carried out in an electro-hydraulic, closed-loop, 97-kN load frame with dual servo-valves. The two servo-valves had volume flow rates of 9×10^{-4} m^3/s and 6.3×10^{-4} m^3/s, respectively. Tests at rates from about 130 to 1000 s^{-1} were done in a Kolsky bar, also called a split Hopkinson pressure bar. In the load frame, data from tests at rates of 10^{-1} s^{-1} or less were recorded with a computer. All data from tests at faster rates were recorded by digital oscilloscopes and transferred to a computer for subsequent manipulation, reduction, and plotting.

The Kolsky bar has been described in detail [1,2,3,4] and therefore it is only briefly mentioned here. The one used in this study is comprised of two titanium alloy bars, 25 mm in diameter and of lengths 1.46 m and 3.54 m, aligned coaxially with the sample sandwiched between them. The bars are held in alignment by low-friction bearings. Samples are held in place by a thin layer of vacuum grease or molybdenum disulfide lubricant applied to the ends. A striker bar, 25 mm in diameter and 152 mm long, composed of the same material as the bars, is launched by the release of compressed nitrogen down a smoothbore gun barrel to impact the end of one of the bars, called the incident bar. The striker bar velocities used in this study were generally less than about 30 m/s. Following impact, a stress wave of approximately constant amplitude and of wavelength equal to twice the length of the striker bar propagates down the incident bar passing a strain gauge before impinging on the sample. Part of the incident wave

is reflected and part passes through the interface into the sample. When reaching the distal end of the sample some of the wave is reflected back into the sample and the remainder passes into the second or transmitter bar. Waves travel back and forth in the sample with a component passing into the transmitter bar at each reflection that superposes to form the wave in the transmitter bar, which passes a second strain gauge. It is shown below how analysis of the strain–time data from the two strain gauge stations is used to compute the stress–strain history of the sample.

The material used in this study was non-welded, ash-fall tuff from the Department of Energy's Nevada Test Site. Test specimens were cored parallel to the axis of a 152-mm core drilled parallel to bedding. Specimens were air-dry or saturated with water. The porosity of the tuff was estimated to be about 30–35% and the measured mean density was 1.700 Mg/m^3 with standard deviation of 0.103. The average ultrasonic longitudinal wave velocity of four specimens of dry tuff was 2.54 $mm/\mu s$. The wave velocity was not measured on the saturated samples. Poisson's ratio was not measured on the dry samples, but for 5 water-saturated specimens it averaged 0.2; this value is consistent with measurements made previously on dry specimens from the same material. These values give a calculated bar wave velocity of 2.41 $mm/\mu s$.

All samples used in the compression frame were right circular cylinders ground in a centerless grinder to about 25 mm in diameter and 50 mm long. Ends were ground flat, perpendicular to the axis, and parallel to each other to within better than 0.001 rad. Several sizes of samples were tested in the Kolsky bar. The length and the length-to-diameter ratio are circumscribed by the requirements of the device and the data analysis. For example, higher strain rate can be achieved and stress analysis is more accurate with shorter samples; however, friction effects on the ends of the samples are alleviated by the use of longer samples. Thus, the sample size and length-to-diameter ratios need to be optimized for each material [5]. In this test series samples were 12.5 mm in diameter and either 12.5 or 25 mm in length, or they were 25 mm in diameter and 25 mm in length. Most samples reported here had length-to-diameter (L/D) ratios of 1.0 but some samples with L/D=2.0 were tested to check for L/D-effects, none were evident for these ratios. However, three samples having L/D=0.5 exhibited much higher strengths than the other L/D ratios. This increased strength most likely resulted from the confinement of the sample by end conditions at the bar/sample interface. These data are not included in this report.

2.1 Reduction of Kolsky Bar Data

Details of typical Kolsky bar data are shown in Figure 1. The strain histories at the two strain gauges are shown, with the record from the transmitter bar shifted

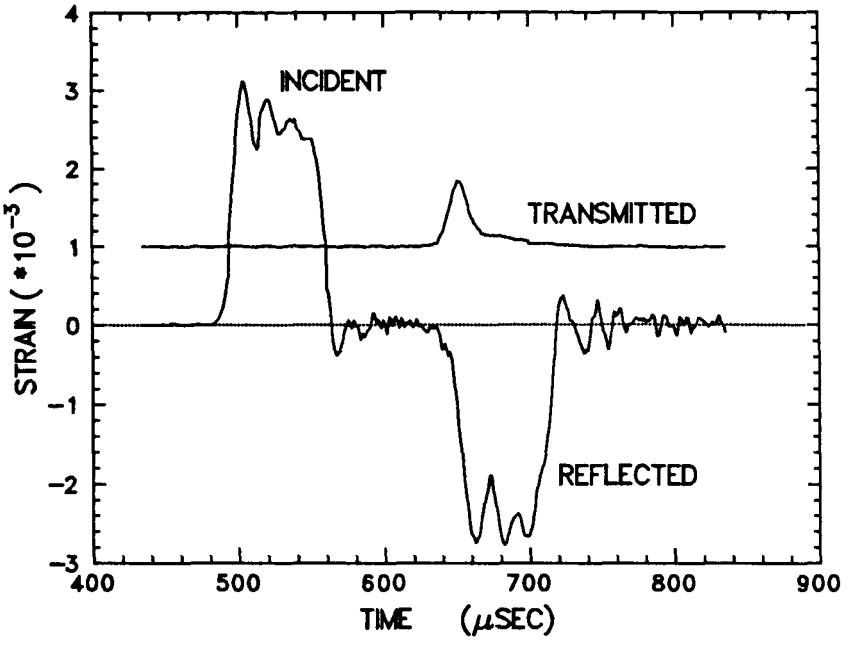

Figure 1: Oscilloscope traces of the two strain gauge stations. The trace of the transmitted wave has been shifted upward by 10^{-3} for clarity.

upward by 1.0×10^{-3} for clarity. As mentioned above, the incident wave is partially reflected as a tensile wave at interface 1, between the incident bar and the specimen. The strain history at the gauge on the transmitter bar is proportional to the stress history experienced by interface 2, between the specimen and the transmitter bar. The oscillations following the leading edges of the incident and reflected waves are most likely due to Pochammer-Chree vibrations [2]. It has been shown how to correct Kolsky bar records for these [6], but because brittle materials fail during the initial rise in the incident wave, and, because these waves are not transmitted through the specimen, no correction was attempted here.

For stress-strain-time calculations, the three waves are shifted on the time-axis to the same zero. The analysis has been shown before [1,2,3] but because a slight variation was used in this study it is briefly reviewed here. The displacements, ξ_1 and ξ_2, at interfaces 1 and 2 are

$$\xi_1 = c_0 \int_0^t (\epsilon_I - \epsilon_R)\, dt' \tag{1}$$

$$\xi_2 = c_0 \int_0^t \epsilon_T\, dt', \tag{2}$$

where ϵ_I, ϵ_R, and ϵ_T, are the incident, reflected, and transmitted strain waves, respectively, and c_0 is the compressional bar wave velocity. The strain ϵ_s in the sample of length l_0 is then

$$\epsilon_s = \frac{\xi_1 - \xi_2}{l_0} = \frac{c_0}{l_0} \int_0^t (\epsilon_I - \epsilon_R - \epsilon_T)\, dt'. \tag{3}$$

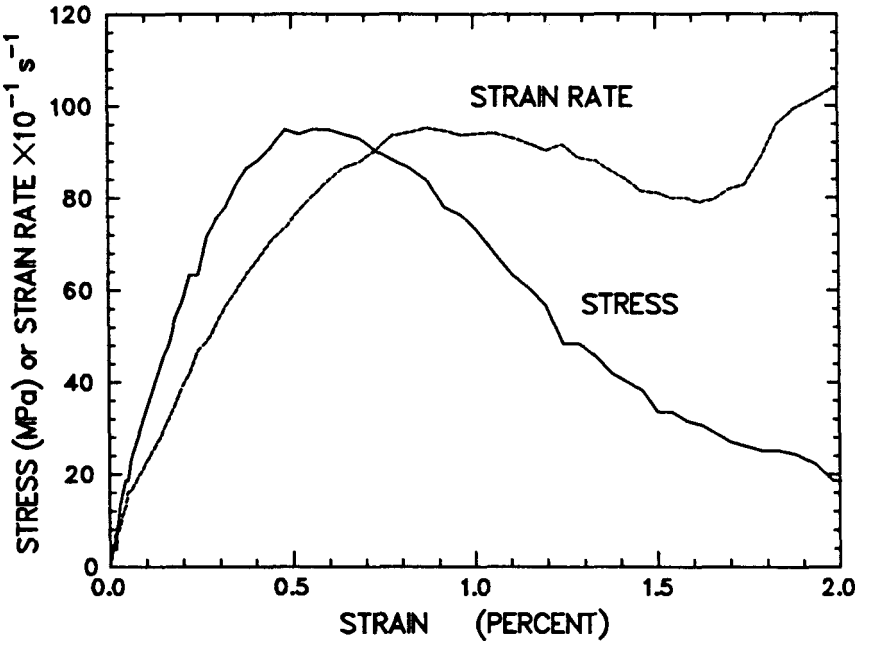

Figure 2: Calculated stress and strain rate plotted against strain.

For cross-sectional area of the bar A and of the specimen A_s, the average stress in the specimen is $\sigma_s = E(A/A_s)\epsilon_T$. Ideally, Equation (3) should be used to compute strain if all three strain histories are measured. However, because ϵ_R tended to be noisy, possibly due to dispersive wave propagation effects, it was assumed that the stress was uniform in the sample so that $\epsilon_R = \epsilon_T - \epsilon_I$. Then,

$$\epsilon_s = \frac{2c_0}{l_0} \int_0^t (\epsilon_I - \epsilon_T)\, dt' . \tag{4}$$

3 Analysis of the Results

Typical stress-strain-time data for the air-dry tuff obtained from the Kolsky bar are plotted in Figure 2. Stress-strain curves at all rates, including the quasistatic, have the same general appearance. Most samples failed at compressive strains near 0.5%. Mean times to peak stress in the Kolsky bar tests were 22 μs for the samples 25.4 mm in length, and 18.5 μs for the samples 12.5 mm in length. The stress wave therefore traversed the longer samples 2 to 3 times and the shorter samples 3 to 4 times before peak stress. Thus, for the shorter samples the number of reflections approaches the requirements for uniform stress, but not for the longer ones. Nevertheless, since the strengths of the longer samples are similar to the shorter samples at equivalent strain rates, it is here assumed that the data from the longer samples are valid.

In the Kolsky bar tests, the strain rate is generally still rising when the ultimate

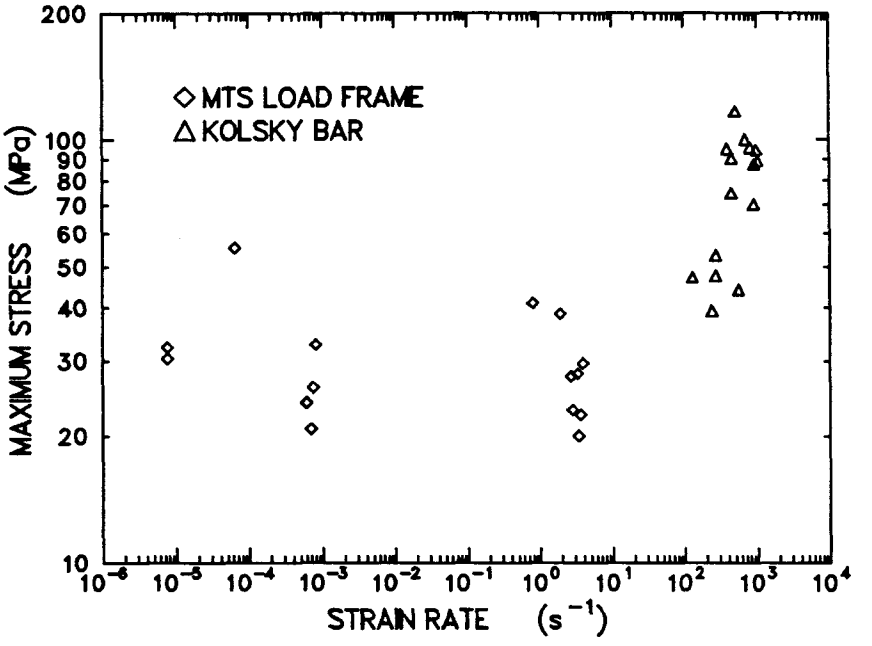

Figure 3: Maximum stress as a function of strain rate at maximum stress for dry tuff.

stress is reached, and I have chosen the value of strain rate at peak stress to characterize the strain rate of the test. Because of the assumptions on which the analysis is based, the early-time strain calculation is inaccurate and therefore the slope of the stress-strain curve is not a good measure of Young's modulus. For tests conducted in the load frame, the strain rate was servo-controlled and was constant for each test.

The ultimate stress, or strength, of air-dry tuff in uniaxial stress compression is plotted against strain rate in Figure 3. There is a great deal of scatter in the strength at a given strain rate for all rates. But it is clear that strength is only a weak function of strain rate below about 100 s^{-1} and that for higher rates strength increases rapidly with increasing rate.

The scatter in strength was suspected to be the result of differences in porosity, ϕ, as found in other studies on tuff [7,8]. Porosity had not been measured on these samples, but bulk densities, ρ, were available. The samples were all taken from the same core drilled along bedding for distances of less than 1 m. Therefore, the mineralogy is probably constant, so that the bulk density is a simple function of porosity, $\rho(\phi)$. Account was taken of the variations in density as follows. The strength of tuff, σ, is known to be a function of the porosity, ϕ, and to some degree the strain rate, $\dot{\epsilon}$, as well as other variables such that

$$\sigma = \sigma(\rho(\phi), \dot{\epsilon}, \ldots). \tag{5}$$

Whence, for uniform test conditions such that all other differentials are zero,

$$d\sigma = \frac{\partial \sigma}{\partial \rho} d\rho + \frac{\partial \sigma}{\partial \dot{\epsilon}} d\dot{\epsilon}. \tag{6}$$

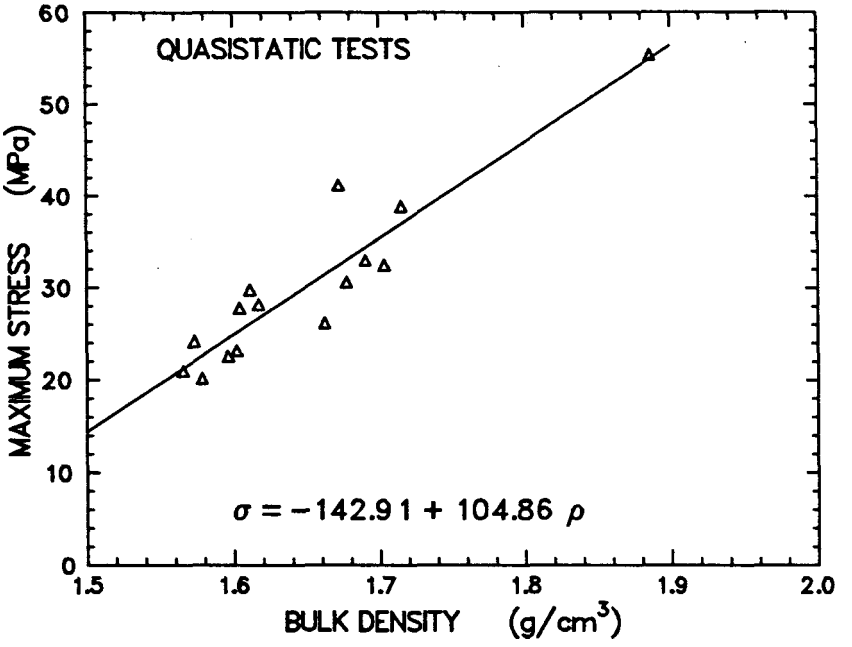

Figure 4: Maximum stress plotted against bulk density. Line determined by linear regression.

Over the strain-rate range 10^{-6} to 10^{-1} s^{-1} , the effect of $\dot{\epsilon}$ on strength is relatively very small compared with that at rates greater than 100 s^{-1} ; thus, it is assumed justifiable to take $\partial\sigma/\partial\dot{\epsilon} = 0$. Therefore, to dominant order $d\sigma = (\partial\sigma/\partial\rho)\, d\rho$. Strength of air-dry tuff for the slow rates is plotted against density in Figure 4 and is seen to be a strong function of the bulk density. Linear regression provides the estimate of $\partial\sigma/\partial\rho = 104.9$. The strength at any density is then corrected to the strength at the mean density by subtracting $(\partial\sigma/\partial\rho)\Delta\rho$, where $\Delta\rho$ is the difference between the measured and the mean densities for a given sample.

Next, it is assumed that the density effect is independent of strain rate, and the strength, corrected for density variations, is plotted (Figure 5) against strain rate for the whole range tested. A reduction in the amount of scatter in the strengths allows a clearer assessment of the relationship between strain rate and strength. The lines are least square fits of log strength to log strain rate separately over the ranges $10^{-6} - 10^{1}$ s^{-1} and $10^{1} - 10^{3}$ s^{-1} . The resulting exponents are also shown. The intersection of the two fitted lines gives $\dot{\epsilon}^* = 82$ s^{-1} , where $\dot{\epsilon}^*$ is the critical strain rate. For $\dot{\epsilon} < \dot{\epsilon}^*$, $\sigma \propto \dot{\epsilon}^{0.007}$, and for $\dot{\epsilon} > \dot{\epsilon}^*$, $\sigma \propto \dot{\epsilon}^{0.35}$.

The strength of the saturated samples is also shown in Figure 5. Above about 22 s^{-1} the strength of saturated tuff is the same as the dry tuff's. Below that rate the saturated tuff is much weaker at all strain rates and, with an exponent of 0.008, exhibits essentially the same rate sensitivity.

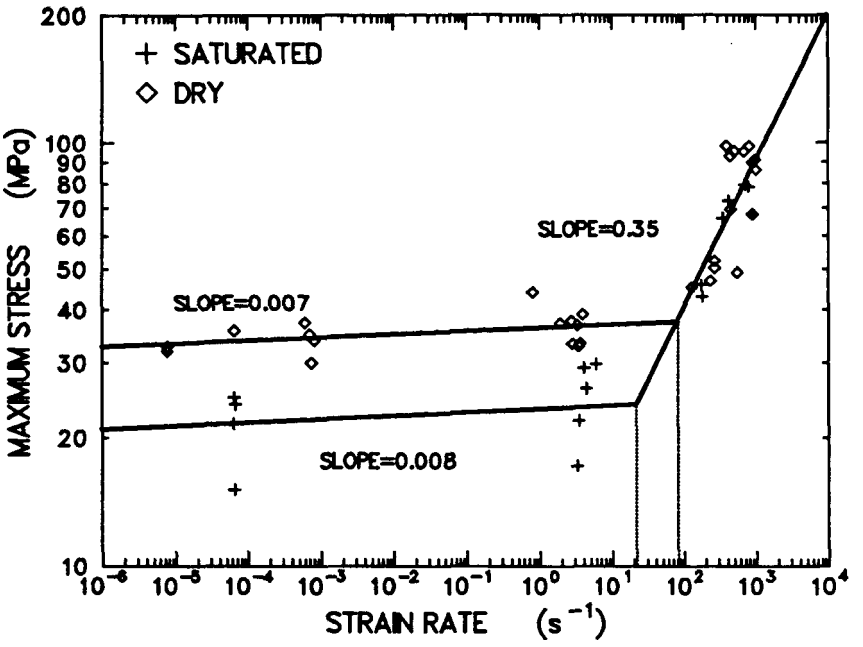

Figure 5: Maximum stress corrected to the mean density plotted against strain rate at maximum stress. Data for dry and saturated tuff combined.

Fragment size data were not collected in this study, but a relationship between fragment size and strain rate was visually apparent. At strain rates below several hundred per second, the samples were broken into about a half dozen pieces plus fines, at high rates closer to 1000 s^{-1} the samples were completely demolished. It was rare to find pieces larger than 1 or 2 mm, and much of the material was reduced to dust.

4 Discussion

The effect of strain rate on rock strength over various subsets of the range 10^{-8} to 10^{-1} s^{-1} has been the subject of many studies for nearly three decades [see refs. in 9]. The first results of dynamic fracture experiments on rock were reported by Kumar [10]. Over the next decade several applications of the Kolsky bar to rock [11,12,13,14,15] appeared, including torsional variations of this device [16] and tests with superimposed confining pressure [17]. The present study appears to be the first in which the effect of saturation was included.

Several authors have observed that when strain rates exceed a certain value, the strength rises rapidly with further increases in rate [10,14]. This has been attributed to inertial confinement effects [18] leading to the achievement of uniaxial strain loading conditions [19]. Direct measurement of the magnitude [20] of the radial acceleration suggests that this effect is negligible. It has also been suggested that the strengthening

observed at high rates is a machine inertia effect, but this appears to be peculiar to a particular apparatus [21]. Moreover, the phenomenon of rapid strengthening with increasing rate above a certain strain rate has been observed in both compression and tension for some rate-sensitive metals [3]. One might reasonably inquire whether either the existence or magnitude of the critical strain rate found in this study is related to the change from one test technique to the other. At this time it can only be stated that the tuff approximately meets the requirements for a valid Kolsky bar test. This implies that deformations are quasistatic in both test types. Also, there is no discontinuity in peak stress as a function of strain rate, which might be expected if the change in techniques were to be significant. Finally, in one study [14], strengths obtained from a Kolsky bar varied continuously with strain rate across the critical strain rate region and merged smoothly with data from a conventional compression testing device.

In reviewing data on a variety of rocks and concrete Grady and Lipkin [22] found that for strain rates greater than about 100 s^{-1} several rocks show a cube root dependence of strength on strain rate. This led Grady and Kipp [23] to develop a theory of dynamic fracture of brittle materials that predicts $\sigma \propto \dot{\epsilon}^{1/3}$. Lankford [24], considering strong ceramics and rocks, combined the dynamic results with quasistatic results and suggested the following functional form for the strength *vs.* strain rate relation:

$$\sigma \propto \begin{cases} \dot{\epsilon}^{1/(1+n)} & \text{if } \dot{\epsilon} < \dot{\epsilon}^* \\ \dot{\epsilon}^{1/3} & \text{if } \dot{\epsilon} > \dot{\epsilon}^* \end{cases} \tag{7}$$

Here n is the exponent in the fracture mechanics relation

$$V \propto K^n \tag{8}$$

where V is the crack growth velocity and K is the stress intensity.

For $\dot{\epsilon} < \dot{\epsilon}^*$, the results presented here indicate $\sigma \propto \dot{\epsilon}^{0.007}$ for dry tuff, and $\sigma \propto \dot{\epsilon}^{0.008}$ for wet tuff. Equation (7) suggests that $n \approx 142$. There appear to be no direct data on n for tuff, but $n = 130$ for a micrite [25], 169 for a basalt [25], and 143 for a limestone [24]. Given the scatter that remains in the data even after correction for density differences, the exponent 0.35 for $\dot{\epsilon} > \dot{\epsilon}^*$ seems to agree with the Grady-Kipp [23] model of dynamic strength.

In the Grady-Kipp inherent flaw model [23], the statistical distribution of flaw sizes is a key element; for reasonable choices of the input variables their model is consistent with the $\dot{\epsilon}^{1/3}$ dependence for dynamic loading. At strain rates less than $\dot{\epsilon}^*$, the applied stress rate is accommodated by a variable rate of crack extension over a limited number of cracks. However, because the rate of crack extension is bounded, above $\dot{\epsilon}^*$ more cracks have to be activated to accommodate the dynamic stress changes. This accounts

for the more pervasive fracturing and consequent smaller fragment sizes produced at higher strain rates. This also suggests [D. Grady, personal communication, 1988] that the critical strain rate, $\dot{\epsilon}^*$, is related to the dimension of the sample. If the sample is being strained at a rate that can be just accommodated by the propagation of one or a very few cracks, then the failure time should be commensurate with the time for a crack to propagate across the sample at its limiting velocity. Because this time is shorter for a smaller sample, the ultimate stress is reached before the $\dot{\epsilon}^{1/3}$-regime is achieved, thus raising the critical strain rate. Taking the maximum tensile crack velocity of 0.38 times the bar wave velocity [26], $v_b = 2.41$ mm/μs, we have $v_{crack} = 0.92$ mm/μs. For samples of length 25.4 mm this predicts a failure time $\tau_f = 27.6$ μs, very close to the observed value of 26 μs. Thus, the micromechanics of the strain rate-effect on peak stress seems to be at least partially understood [22,23,24].

The effect of water saturation on the strain-rate sensitivity may be a clue to the mechanisms of deformation. The strength reduction from air-dry to saturated at a given rate is believed to be mostly mechanical and not a result of chemical process such as hydrolytic weakening because the air-dry samples do have adsorbed water in equilibrium with the prevailing humidity. For this porous, saturated rock it may be that at strain rates less than critical, the pore pressure increases with increasing strain because of collapse of pores combined with low permeability. This increase in pore pressure would cause reduced strength compared to the dry samples in accordance with the effective stress principle. At strain rates greater than critical, the water cannot flow fast enough to keep pores and cracks saturated, and thus the increased pore pressures do not develop. With no increase in pore pressure, the effective stresses are the same in the dry and saturated samples leaving the strength unaffected by the presence of water.

5 Conclusions

The unconfined compressive strength of a porous, ash-fall tuff has been measured as a function of strain rate from 10^{-6} to 10^{3} s^{-1} . A substantial portion of the scatter in the strength at a given strain rate was attributed to variations in bulk density (porosity). When the observed strengths were corrected for variations due to density variations, they became a well-defined function of the strain rate. Over the range from 10^{-6} to 82 s^{-1} , the strength is a weak function of rate; it is proportional to the strain rate raised to the power 0.007. Above 82 s^{-1} the strength is proportional to the cube root of the strain rate. These data are consistent with the concept that for slower rates the rate effect is a function of the crack propagation velocity *vs.* stress-intensity-factor relationship [23]. At high rates the upper limit of the strain rate effect is encountered and strength is controlled by an inertial crack model [22].

Acknowledgement—I drew heavily upon Larry Costin's expertise in the area of Kolsky bar testing, and used his computer program to reduce the data. I thank David Holcomb for suggesting an important improvement in the analysis of the density data, and Dennis Grady, Wolfgang Wawersik and David Zeuch for careful reviews. Mark Stavig assisted with the experiments.

6 References

1. Kolsky, H., An investigation of the mechanical properties of materials at very high rates of loading, *Proc. Phys. Soc.* **B62**, 676–700 (1949).

2. Kolsky, H., *Stress Waves in Solids*, Chap. 4. Dover, New York (1963).

3. Lindholm, U.S., and L.M. Yeakley, High strain-rate testing: tension and compression, *Exp. Mech.* **8**, 1–9 (1968).

4. Lindholm, U.S., Some experiments with the split Hopkinson pressure bar, *J. Mech. Phys. Solids* **12**, 317–335 (1964).

5. Bertholf, L.D., and C.H. Karnes, Two-dimensional analysis of the split Hopkinson pressure bar system, *J. Mech. Phys. Solids* **23**, 1–19 (1975).

6. Follansbee, P.S., and C. Frantz, Wave propagation in the split Hopkinson pressure bar, *J. Eng. Mat. and Technology* **105**, 61–66 (1983).

7. Olsson, W.A., Rock mechanics properties of volcanic tuffs from the Nevada Test Site, *Tech. Rept. SAND80-1453*, Sandia National Laboratories, Albuquerque, NM (1980).

8. Price, R.H., and S.J. Bauer, Analysis of the elastic and strength properties of Yucca Mountain tuff, Nevada, in *Research & Engineering Applications in Rock Masses*, Proc. 26^{th} U.S. Symp. of Rock Mech., ed. E. Ashworth, Balkema, Boston pp. 89–96 (1985).

9. Paterson, M.S., *Experimental Rock Deformation–The Brittle Field*, p. 28, Springer-Verlag, New York (1978).

10. Kumar, A., The effect of stress rate and temperature on the strength of basalt and granite, *Geophysics* **33**, 501–510 (1968).

11. Hakalehto, K.O., Brittle fracture of rocks under impulse loads, *Int. J. Frac. Mech.* **6**, 249–256 (1970).

12. Lankford, J., Dynamic strength of oil shale, *J. Soc. Pet. Engrs.* **16**, 17–22 (1977).

13. Lindholm, U.S., L.M. Yeakley, A. Nagy, The dynamic strength and fracture properties of Dresser basalt, *Int. J. Rock Mech. Min. Sci. & Geomech. Abstr.* **11**, 181–191 (1974).

14. Green, S.J., and R.D. Perkins, Uniaxial compression test at varying strain rates on three geologic materials, in 10^{th} *Symp. on Rock Mechanics*, 35–54, Soc. Min. Eng. AIME (1970).

15. Goldsmith, W., J.L. Sackman, C. Ewert, Static and dynamic fracture strength of Barre granite, *Int. J. Rock Mech. Min. Sci. & Geomech. Abstr.* **13**, 303–309 (1976).

16. Lipkin, J., D.E. Grady, and J.D. Campbell, Dynamic flow and fracture of rock in pure shear, *18th U.S. Symp. on Rock Mech.*, Keystone, CO, 3B2-1 (1977).

17. Green, S.J., J.D. Leasia, R.D. Perkins, and A.H. Jones, Triaxial stress behavior of Solenhofen limestone and Westerly granite at high strain rates, *J. Geophys. Res.* **77**, 3711–3724 (1972).

18. Janach, W., The role of bulking in brittle failure of rocks under rapid compression, *Int. J. Rock Mech. Min. Sci. & Geomech. Abstr.* **13**, 177–186 (1976).

19. Brace, W.F., and A. H. Jones, Comparison of uniaxial deformation in shock and static loading of three rocks, *J. Geophys. Res.* **76**, 4913–4921 (1971).

20. Malvern, L.E., T. Tang, D.A. Jenkins, and J.C. Gong, Dynamic comressive strength of cementitious materials, in *Cement-Based Composites: Strain Rate Effects on Fracture*, Mat. Res. Soc. Symp. Proc. **64**, eds. S. Mindess and S.P. Shah, pp. 119–138 (1986).

21. Blanton, T.L., Effect of strain rates from 10^{-2} to 10 sec^{-1} in triaxial compression tests on three rocks, *Int. J. Rock Mech. Min. Sci. & Geomech. Abstr.* **18**, 47–62 (1981).

22. Grady, D.E., and J. Lipkin, Criteria for impulsive rock fracture, *Geophys. Res. Let.* **7**, 255–258 (1980).

23. Grady, D.E., and M.E. Kipp, Dynamic rock fragmentation, in *Fracture Mechanics of Rock*, ed. B.K. Atkinson, pp. 429–475, Academic Press Inc., London (1987).

24. Lankford, J., The role of tensile microfracture in the strain rate dependence of compressive strength of fine-grained linestone—analogy with strong ceramics, *Int. J. Rock Mech. Min. Sci. & Geomech. Abstr.* **18**, 173–175 (1981).

25. Atkinson, B.K., P.G. Meredith, Experimental fracture mechanics data for rocks and minerals, in *Fracture Mechanics of Rocks*, pp.477–525, ed. B.K. Atkinson, Academic Press, New York (1987).

26. Roberts, D.K., and A.A. Wells, Velocity of brittle fracture, *Engineering* **178**, 820-821 (1954).

DISTRIBUTION LIST

D. F. Patch
Pacifica Technology
Post Office Box 148
Del Mar, CA 92014

N. Rimer
S-Cubed
Post Office Box 1620
La Jolla, CA 92038

C. F. Peterson
S-Cubed
Post Office Box 1620
La Jolla, CA 92038

P. S. DeCarli
SRI International
333 Ravenswood Ave.
Menlo Park, CA 94025

J. Duffy
Division of Engineering
Brown University
Providence, RI 02912

Fred App
Los Alamos National Laboratories
M/S 659
P.0. Box 1663
Los Alamos, NM 87543

John Rambo
L200
Lawrence Livermore National
Laboratories
P.O. Box 808
Livermore, CA 94550

Byron Ristvet
Defense Nuclear Agency
P.O. Box 98539
Las Vegas, NV 89193-8539

1510 J. W. Nunziato
1520 L. W. Davison
1521 R. D. Krieg
1523 E. P. Chen
1530 D. B. Hayes
1533 P. Y. Yarrington
1534 J. R. Asay
1534 D. E. Grady
3141 S. A. Landenberger (5)
3154-1 C. L. Ward (8) for DOE/OSTI
3151 W. I. Klein (3)
6240 W. C. Luth
6241 H. C. Hardee
6242 S. R. Brown
6242 D. J. Holcomb
6242 W. A. Olsson (10)
6242 L. W. Teufel
6242 W. R. Wawersik
6242 D. H. Zeuch
6243 T. M. Gerlach
7110 J. D. Plimpton
7111 A. J. Chabai
7112 C. W. Smith (5)
7116 R. P. Reed
8524 J. A. Wackerly